Journal of Solid State Chemistry **165,** 136–147 (2002)
doi:10.1006/jssc.2002.9516, available online at http://www/idealibrary.com on IDEAL®

The Disordered High-Temperature Structure of $(NH_4)_3H(SO_4)_2$ and Its Relationship to the Room-Temperature Phase

K. Friese[1] and M. I. Aroyo

Departamento de Física de la Materia Condensada, Universidad del País Vasco, Apdo. 644, Bilbao, Spain
E-mails: k.friese@fkf.mpg.de; wmpararm@lg.ehu.es

and

L. Schwalowsky, G. Adiwidjaja, and U. Bismayer

Mineralogisch-Petrographisches Institut, Universität Hamburg, Grindelallee 48, 20146 Hamburg, Germany
E-mails: adiwid@aedcad4.psych1.uni-hamburg.de; ubis@mineralogie.uni-hamburg.de

Received September 17, 2001; in revised form January 8, 2002; accepted January 25, 2002

The structure of letovicite, $(NH_4)_3H(SO_4)_2$ has been redetermined at 293 and 420 K. At room temperature the structure crystallizes monoclinic, space group $C12/c1$ (no. 15), with lattice parameters $a = 15.418(5)$ Å, $b = 5.905(5)$ Å, $c = 10.223(5)$ Å and $\beta = 102.806(5)^\circ$. The structure is composed of two symmetrically independent isolated NH_4^+ tetrahedra and $[SO_4–H–SO_4]^{3-}$ dimers with a symmetrical hydrogen bond connecting the two sulfate tetrahedra. At 420 K the structure is rhombohedral, space group $R\bar{3}m$ (no. 166) with lattice parameters $a = 5.9039(5)$ and $c = 22.5360(6)$ Å. While the low-temperature phase is completely ordered, this does not hold for the high-temperature phase: the hydrogen and oxygen atoms which constitute the hydrogen bond are disordered with the consequence that the hydrogen bond is now strongly asymmetric. Furthermore, the hydrogen atoms in one of the two symmetrically independent NH_4^+ tetrahedra are disordered and have probably some share in the high protonic conductivity which has so far been attributed mainly to the hydrogen atom of the hydrogen bond. © 2002 Elsevier Science (USA)

Key Words: **letovicite; $(NH_4)_3H(SO_4)_2$; high-temperature phase; disorder; symmetry mode analysis.**

1. INTRODUCTION

Letovicite, $(NH_4)_3H(SO_4)_2$, belongs to a family of compounds with general formula $M_3H(BO_4)_2$ ($M = K^+$, Rb^+, Cs^+, NH_4^+; $B = S^{2-}$, Se^{2-}) in which ferroic phase transitions commonly occur. For the triammonium hydrogen sulfate, the transition sequence

$$\text{Phase I} \xrightarrow{413\,K} \text{Phase II} \xrightarrow{265\,K} \text{Phase III} \xrightarrow{141K} \text{Phase IV} \xrightarrow{133\,K} \text{Phase V} \xrightarrow{63\,K} \text{Phase VI}$$

has been observed (1–3). Furthermore, DSC and electronic conductivity measurements carried out by Fukami *et al.* (4) showed an anomaly at 463 K and the authors proposed another phase transition at this temperature.

No complete structural determinations have been carried out for phases III–VI. Yet, according to X-ray diffraction studies carried out by Chen *et al.* (5), the space groups are probably $P12/n1$ or $P1n1$ for phase III and $C121$, $C1m1$ or $C12/m1$ for phase IV with a unit cell volume comparable to phase II. In contradiction to this, Kamouni *et al.* (6) described a doubling of the volume of the unit cell of phase III with respect to phase II and determined extinction rules in agreement with the possible space groups $P12/c1$ or $P1c1$.

The structure of phase II is well known. It was first determined by Suzuki and Makita (7) and later confirmed by Leclaire *et al.* (8). At room temperature, the lattice parameters given in Ref. (8) are $a = 15.435(2)$Å, $b = 5.865(1)$ Å , $c = 10.1696(8)$ Å and $\beta = 101.829(8)^\circ$, space group $C12/c1$.

The structure is characterized by sulfate tetrahedra which are linked via a common symmetric hydrogen bond and form dimers of composition $[SO_4–H–SO_4]^{3-}$. These dimers together with one of the symmetrically independent NH_4^+ tetrahedra form layers of composition $[(NH_4)_2H_2(SO_4)_4]^{4-}$ parallel to the b,c plane of the monoclinic phase (i.e., the a,b plane of the rhombohedral

[1]To whom correspondence should be addressed. Present address: Max-Planck Institut für Festkörperforschung, Heisenbergstr. 1, D-70569 Stuttgart, Germany. Fax: +00 49 711 689-1502.

0022-4596/02 $35.00

phase). Other layers composed of isolated [NH_4^+] tetrahedra alternate with them and provide the necessary charge balance.[2]

The high-temperature phase I of $(NH_4)_3H(SO_4)_2$ is of special interest due to its elevated protonic conductivity (9). Two independent structure determinations have been carried out. Following Ref. (10) the structure at 430 K is rhombohedral, space group $R\bar{3}$ with lattice parameters $a = 5.907(2)$ Å and $c = 22.549(7)$ Å while according to Ref. (11) who determined the structure at 413 K with powder diffraction methods the space group is $R\bar{3}m$ with lattice parameters $a = 5.906(1)$ Å and $c = 22.602(1)$ Å.

In view of these contradictions (which will be discussed in more detail in the section "structure refinement and space group") and the importance of a correct structural model to understand the protonic conductivity of the high-temperature phase, we thought it prudent to carry out a new structural analysis.

2. EXPERIMENTAL

The crystals of letovicite, $(NH_4)_3H(SO_4)_2$, were grown according to the method described by Gesi (1). The intensities of the reflections were measured at 293 and 420 ± 5 K with an automatic single-crystal diffractometer CAD4 and monochromated Mo$K\alpha$ radiation. For heating the device described in Ref. (12) was used which was calibrated using a calcite crystal and corresponding lattice parameters given by Rao *et al.* (13). As the crystals of letovicite are hygroscopic they were enclosed in capillaries.

For the measurement of diffraction intensities, the monoclinic setting $C12/c1$ with the corresponding lattice parameters (see Table 1) was used at both temperatures. The data collection at high temperatures was limited in time because thermally induced decomposition appeared to take place after long heating times. This was reflected in the fact that the standard reflections for the measurement at 420 K showed a slight decrease of approximately 7% and it was necessary to correct intensities accordingly. Lattice parameters as well as further details concerning the measurement are given in Table 1.

3. STRUCTURE REFINEMENT AND SPACE GROUP

According to a single-crystal structure refinement carried out by Fukami *et al.* (10) the high-temperature phase of letovicite is trigonal, space group $R\bar{3}$ with lattice parameters $a = 5.907(2)$ Å and $c = 22.549(7)$ Å. The authors assumed the chosen space group to be the correct one in analogy with one of the phases of the related compound $(NH_4)_3H(SeO_4)_2$. Anyhow, in contrast to $(NH_4)_3H(SO_4)_2$ in the selenate, two trigonal phases with space groups $R\bar{3}$ and $R\bar{3}m$ are observed and the authors do not give convincing arguments as to why they prefer the lower symmetrical space group. Furthermore, a close look at the atomic coordinates published reveals that the heavy atoms do not violate the higher symmetry of $R\bar{3}m$ but are clearly within the experimental error consistent with this space group. For the oxygen atoms O(1) close to the Wyckoff position 6*c* (0,0,*z*), the authors assume disorder and a split atom model (with presumably $\frac{1}{3}$ of the ideal occupation of the corresponding position) was used in the refinement. All of the positions of the hydrogen atoms are given though unfortunately, it is not clear as to whether they were taken from difference Fourier synthesis or were merely calculated using geometrical criteria. Furthermore, the hydrogen atoms have to be disordered also, as the authors give a total of 66 hydrogen atoms in the unit cell (while 39 is the correct value). Unfortunately, no details about the occupation factors of the hydrogen positions are given and the distribution of the 39 H atoms over the 66 possible positions is not clearly stated. Anyhow, for geometrical reasons, we assume that the hydrogen positions (denoted H(4) and H(5)) around one of the N(2) nitrogen atoms (in position 0, 0, *z*) are completely occupied while the other three positions involve disorder. For the hydrogen atom H(1) which forms the hydrogen bond, the real occupation should be $\frac{1}{6}$ of the ideal one (resulting in three positions per unit cell) and for the two hydrogen atoms H(2) and H(3) forming the tetrahedral around N(1), we assume $\frac{1}{2}$ of the ideal occupation.

In the X-ray powder diffraction studies of Ref. (1), on the other hand, the space group $R\bar{3}m$ was assumed to be the correct one. The authors also introduce a split atom position, but in this case it is not the oxygen atom O(1) on Wyckoff position 6*c* (of $R\bar{3}m$) which is disordered, but the position 36*i* (*x*, *y*, *z*) corresponding to atom O(2,3,4) of the monoclinic phase is supposed to be only half occupied.

Considering the contradictions about the real space group and the existing type of disorder in the crystal, we took special care in the refinement process. Thus, we tried refinement in different space groups and took into account possible twin models. In our refinements, we only used the more securely determined heavy atom positions and in the beginning neglected the hydrogen atoms. The results of these refinements are listed in Table 2.

As possible space groups we tried $C1c1$, $C12/c1$ (corresponding to the symmetry of the low-temperature structure), $R3$, $R\bar{3}$, $R32$, $R3m$ and $R\bar{3}m$. For the acentric space groups we also tried refinement as inversion twins. It is evident that the monoclinic space groups are not the correct choices as the reflections corresponding to the

[2]In the following atoms of the hydrogen bond will be denoted O(1) and H(1), other oxygen atoms O(2), O(3) and O(4), nitrogen and hydrogen within the sulfate layer are N(1), H(2) and H(3), and nitrogen and hydrogen of the second layer are N(2), H(4) and H(5).

TABLE 1
Crystal Data and Experimental Conditions

	293 K		420 K
$a_{monoclinic}$ (Å)	15.418(5)		15.406(1)
$b_{monoclinic}$ (Å)	5.905(5)		5.9044(3)
$c_{monoclinic}$ (Å)	10.223(5)		10.2251(6)
$\beta_{monoclinic}$ (°)	102.806(5)		102.784(4)
$V_{monoclinic}$ (Å)	907.6(2)		907.03(10)
Lattice parameters from in 2θ range		25 reflections $18^\circ \leq \theta \leq 37^\circ$	
$a_{rhombohedral}$ (Å)	5.904(5)		5.9039(5)
$c_{rhombohedral}$ (Å)	22.552(5)		22.5360(6)
$V_{rhombohedral}$ (Å^3)	680.8(1)		680.3(1)
$\rho_{calculated}$ (mg/m^3]		1.81	
μ (mm^{-1})		6.13	
Diffractometer		CAD-4	
Wavelength (Å)		1.54184	
Scan		ω–2θ	
Scan angle		$0.8 + 0.35 \sin \theta$	
θ range		$2.7^\circ < \theta < 26.5^\circ$	
hkl_{min}–hkl_{max}	0,0, $\overline{12}$–19,7,12		$\overline{19}$,0, $\overline{12}$-19,7,12
Two standard reflections		Every 120 min	
Crystal size (mm^3)		0.003	
Measured reflections	929		1877
Independent reflections	210		210
$>2\sigma$	193		193
$R(F^2)_{int}$ (%)	5.08		9.12
Structure refinement program		SHELXL97 (14)	
$R(F_{all}) = \sum \lvert F_o \rvert - \lvert F_c \rvert / \sum \lvert F_o \rvert$	0.032		0.035
$R(F_{observed})$	0.034		0.033
$wR(F^2_{all}) = \{\sum[w(F_o^2 - F_c^2)^2] / \sum[w(F_o^2)^2]\}^{1/2}$	0.094		0.083
Diff. density maximum	0.234		0.193
Diff. density minimum	−0.342		−0.172
Extinction correction		SHELXL97 (14)	
Extinction coefficient	0.031(2)		0.0085(11)
Weighting scheme		$w = 1/[\sigma^2(F_{obs})^2 + (aP)^2 + bP]$	
with		$P = (\mathrm{Max}(F^2_{obs}) + 2F^2_{calc})/3$	
a	0.045		0.020
b	0.239		0.488

systematic extinctions of the *R*-lattice are not observed. Furthermore, the twin models led to insignificant volume fractions for the second twin individual and they could also be discarded.

On the other hand, the high anisotropic displacement parameters of atoms O(1) suggested the introduction of a split atom position close to Wyckoff position 6*c*. This clearly led to an improvement of the agreement factors for all space groups and we therefore accepted this position to be correct.

From the rhombohedral space groups tried, the *R*32 models led to slightly worse agreement factors than the other three space groups. Space groups $R\overline{3}$, *R*3*m* and $R\overline{3}m$ give comparable agreement factors. Taking into account the obtained results, we finally considered the split atom model in $R\overline{3}m$ to be the correct one.

Using the refined coordinates and anisotropic displacement factors from this model, we searched for the hydrogen atoms using difference Fourier synthesis and were able to find five different hydrogen positions. When we introduced the corresponding coordinates in the refinement the agreement factors clearly improved. In subsequent cycles, the coordinates of the hydrogen atoms hardly changed and even the refinement of the isotropic displacement parameters led to reasonable values.

Refinement of the room-temperature phase of $(NH_4)_3H(SO_4)_2$ was tried in space groups $C12/c1$ and $C1c1$. As the agreement factors for the acentric space group are not significantly better than for the centric one, we assumed the space group $C12/c1$ to be the correct one. A twin refinement using the threefold axis of the rhombohedral phase as twin element did not lead to significant volume fractions for the second and third twin individuals and was discarded. All of the hydrogen atom positions were found without difficulties in a difference Fourier synthesis. Because of the high pseudosymmetry and to

TABLE 2
Results of the Structure Refinements for $(NH_4)_3H(SO_4)_2$ in Different Space Groups at 420 K; *R*-Values Given in [%]; H-Atoms Are Only Considered in the Last Model of $R\bar{3}m$

Space group		Number parameters	$R(F)>2\sigma$	$R(F)_{all}$	wR(F*2)
$C12/c1$ (no. 15)		61	7.28	8.38	27.55
$C1c1$ (no. 9)		119	9.12	10.38	34.95
R3 (no. 146)		41	6.64	6.98	19.19
$R3$	Split atom	53	5.90	6.28	16.86
$R\bar{3}$ (no. 148)		22	5.43	5.72	15.98
$R\bar{3}$	Split atom	28	4.34	4.61	13.18
$R32$ (no. 155)		22	5.98	6.32	16.70
$R32$	Split atom	28	5.09	5.40	14.00
$R3m$ (no. 160)		35	5.49	5.84	16.30
$R3m$	Split atom	41	4.53	4.84	13.44
$R\bar{3}m$ (no. 166)		19	5.45	5.58	15.31
$R\bar{3}m$	Split atom	20	4.37	4.50	12.44
	Including H-atoms	34	3.34	3.46	8.63

avoid unnecessary correlations we thought it prudent to restrict the isotropic displacement parameters of all the hydrogen atoms to an identical value.

Final coordinates and displacement factors for both temperatures are given in Table 3; selected interatomic distances and angles are listed in Table 4.

TABLE 3
Positional and Equivalent Thermal Displacement Parameters for $(NH_4)_2H(SO_4)_2$ at 293 and 420 K

Atom	x	y	z	Occ.	U_{eq}
		293 K; space group $C12/c1$			
S	0.11419(2)	0.21844(8)	0.46134(4)	1.0	0.0324(3)
N1	0.5	0.2308(5)	0.25	0.5	0.0415(6)
N2	0.19879(12)	0.2750(4)	0.15293(19)	1.0	0.0453(6)
O1	0.01482(8)	0.1851(3)	0.44230(15)	1.0	0.0495(5)
O2	0.15028(9)	0.2228(3)	0.60524(13)	1.0	0.0507(4)
O3	0.12875(8)	0.4325(3)	0.39863(14)	1.0	0.0530(4)
O4	0.14900(8)	0.0275(2)	0.39841(14)	1.0	0.0526(4)
H1	0.0	0.0	0.0	0.5	0.117(6)
H2	0.472(3)	0.160(7)	0.189(4)	1.0	0.117(6)
H3	0.465(3)	0.291(6)	0.272(4)	1.0	0.117(6)
H4	0.253(3)	0.293(7)	0.160(4)	1.0	0.117(6)
H5	0.176(3)	0.365(7)	0.097(4)	1.0	0.117(6)
H6	0.188(3)	0.154(7)	0.116(5)	1.0	0.117(6)
H7	0.185(3)	0.287(6)	0.206(4)	1.0	0.117(6)
		420 K; space group $R\bar{3}m$			
S	0.0	0.0	0.40947(4)	0.16667	0.0594(6)
N1	0.0	0.0	0.0	0.08333	0.0661(19)
N2	0.0	0.0	0.1994(3)	0.16667	0.0755(15)
O1	0.0376(9)	−0.0376(9)	0.3428(2)	0.16667	0.078(4)
O2	0.1352(2)	−0.1352(2)	0.57055(10)	0.5	0.0823(9)
H1	0.5	0.0	0.0	0.08333	0.08(4)
H2	0.082(8)	−0.082(8)	0.014(4)	0.25	0.11(4)
H3	0.039(18)	−0.039(18)	0.964(8)	0.08333	0.06(6)
H4	0.0	0.0	0.161(8)	0.16667	0.18(5)
H5	0.064(11)	−0.064(11)	0.222(2)	0.5	0.31(6)

4. DISORDER IN THE HIGH-TEMPERATURE PHASE

Of the 10 symmetrically independent atomic positions in the high-temperature phase, four show disorder: the two atoms forming the hydrogen bond H(1) and O(1) and the hydrogen atoms which belong to the $N(1)H_4^+$ tetrahedra of the layers containing the sulfate dimers. The basis (O(2)-atoms) and the center (S-atoms) of the sulfate group as well as the atoms of the highly distorted $N(2)H_4^+$ tetrahedra are completely ordered and positions H4 and H5 are fully occupied (see Table 3).

The most important contribution to the disorder in the structure results from the O(1) atoms which form the top of the sulfate tetrahedra and are involved in the hydrogen bond. Ideally, this oxygen should be on the threefold axis in position 0, 0, z yet it is slightly shifted with a split atom distance of 0.67(2) Å and now occupies the more general position $x, \bar{x}, z$. This implies three possible orientations for the sulfate tetrahedra. Compared to the ideal situation (assuming coordinates 0,0,0.199 for O(1)), this shift leads to a slightly longer S–O distance (1.514(1) Å instead of 1.502 Å). But the effect on the hydrogen bond is probably even more important: in the idealized model, the bond O–H–O is symmetric with a distance of 1.72 Å. The shift of the O(1) atom changes this to a short distance O(1)–H(1) of 1.34(4) Å and a longer bond O(1)···H(1) of 1.94(6) Å.

The hydrogen atom which is involved in the hydrogen bond is also disordered though here no displacement from the ideal position is observed. The Wyckoff position occupied by H(1) is 9*e*, yet only three hydrogen atoms are distributed over the nine possible positions.

For the disordered tetrahedra $N(1)H_4^+$, there are three possible and geometrically reasonable models in the high-symmetry phase:

TABLE 4
Bond Distances for $(NH_4)_3H(SO_4)_2$ at 293 and 420 K

293 K	(Å)	420 K	(Å)
S–O2	1.453(2)	S–O2^{i}	1.454(2)
S–O3	1.470(2)	–O2^{ii}	1.454(2)
S–O4	1.458(2)	–O2^{iii}	1.454(2)
S–O1	1.514(1)	–O1	1.550(5)
	1.474		1.478
		O1–O1^{ii,iii}	0.665(15)
	deg		deg
O2–S–O3	111.61(9)	O2^{i}–S–O2^{ii}	110.86(9)
O2–S–O4	111.39(9)	O2^{i}–S–O2^{iii}	110.86(9)
O3–S–O4	111.65(9)	O2^{i}–S–O1	100.5(2)
O2–S–O1	106.38(8)	O2^{ii}–S–O2^{iii}	110.86(9)
O3–S–O1	107.85(7)	O2^{ii}–S–O1	100.5(2)
O4–S–O1	107.68(8)	O2^{iii}–S–O1	122.4(3)
	(Å)		(Å)
N1–H3	0.71(8)	N1–H2	0.90(8)
N1–H3^{vi}	0.71(8)	N1–H2^{iv}	0.90(8)
N1–H2	0.80(8)	N1–H2^{v}	0.90(8)
N1–H2^{vi}	0.80(8)	N1–H3(H3^{iv},H3^{v})	0.90(8)
	deg		deg
H3–N1–H3^{vi}	120(6)	H2^{iv}–N1–H2^{iv}	108(5)
H3–N1–H2^{vi}	110(6)	H2^{iv}–N1–H2^{v}	108(5)
H3–N1–H2^{vi}	101(6)	H2^{iv}–N1–H3	84(3)
H3^{vi}–N1–H2	110(6)	H2^{iv}–N1–H2^{v}	108(5)
H2^{vi}–N1–H2^{vi}	116(6)	H2^{iv}–N1–H3	121(6)
H2^{vi}–N1–H3	101(6)	H2^{v}–N1–H3	121(6)
	(Å)		(Å)
N2–H6	0.63(9)	N2–H5	0.83(9)
–H4	0.80(9)	–H5^{ii}	0.83(9)
–H5	0.80(9)	–H5^{iii}	0.83(9)
–H7	0.83(8)	–H4	0.87(17)
	deg		deg
H6–N2–H4	112(6)	H5–N2–H5^{ii}	86(2)
H6–N2–H5	116(6)	H5–N2–H5^{iii}	86(2)
H6–N2–H7	116(6)	H5–N2–H4	127(5)
H4–N2–H5	104(6)	H5^{ii}–N2–H5^{ii}	86(2)
H4–N2–H7	104(6)	H5^{ii}–N1–H4	127(5)
H5–N2–H7	104(6)	H5^{iii}–N1–H4	127(5)
	(Å)		(Å)
O1^{vii}–H1	1.28(5)	O1–H1	1.34(4)
O1^{viii} $\cdots$ H1	1.28(5)	O1 $\cdots$ H1	1.94(6)
O1^{vii}–O1^{viii}	2.572(2)	O1–O1	2.674(3)
	deg		deg
O1^{vii}–H1–O1^{viii}	180.0	O1–H1–O1	169.7(9)

Note. (i) $\bar{x}, \bar{y}, 1-z$; (ii) $y, -x+y, 1-z$; (iii) $x-y, x, 1-z$; (iv) $\bar{x}, x-y, z$; (v) $-x+y, \bar{x}, z$; (vi) $1-x, y, \frac{1}{2}-z$; (vii) $\bar{x}, y, \frac{1}{2}-z$; (viii) $x, \bar{y}, -\frac{1}{2}+z$.

- *Model 1*: One symmetrically independent hydrogen atom in the general Wyckoff position 36*i* with $\frac{1}{3}$ of the ideal occupation (= 12 atoms in the unit cell).
- *Model 2*: One symmetrically independent hydrogen atom in Wyckoff position 18*i* with occupation $\frac{1}{4}$ (= 9 atoms) and a second hydrogen atom in Wyckoff position 6*c* i.e., 0,0,*z* with occupation $\frac{1}{3}$ (= 3 atoms).
- *Model 3*: Two symmetrically independent hydrogen atoms in positions 18 h i.e., $x, \bar{x}, z$ one with $\frac{1}{2}$ of the ideal occupation (= 9 atoms) the other with $\frac{1}{6}$ (= 3 atoms).

Naturally with X-ray data, it is difficult to distinguish as to which of the three models is the correct one. But surprisingly the agreement factors are rather sensible to the hydrogen positions and we were even able to refine coordinates and displacement parameter of the hydrogen atoms without major difficulties. The coordinates of H(2) and H(3) which we found in the difference Fourier synthesis and used in the refinement (see Table 3) correspond to Model 3. In this model, there occur six different orientations for the tetrahedra around N(1). A schematic diagram of the six possibilities viewed along the threefold axis is given in Fig. 1. The N(1) atom is drawn as a black circle. The six possible positions of the orbits of H(2) and H(3), respectively, are shown as open circles. To form a coordination polyhedra with approximate tetrahedral geometry, three positions of the orbit of H(2) with identical *z* coordinates must be occupied. These three atoms form the basis of the tetrahedra. The top of the tetrahedra is formed by one hydrogen atom in one of the six possible positions of the H(3) orbit. For each of the two possible sets of three H(2) atoms, there are three different possibilities for choosing the top position of H(3). The reasonable combinations are given in the figure; all other choices of positions do not lead to tetrahedral geometry.

We also tried to refine using hydrogen atom coordinates corresponding to the second model (which basically corresponds to the one given in Ref. (10) in space group $R\bar{3}$). In this model, three of the possible positions of orbit 18i with identical *z* parameters form the basis of the tetrahedra and one of the positions of orbit 6*c* forms the top. Isotropic displacement factors and coordinates of the hydrogen atoms in these positions can be refined. The final *R*-value for this model is comparable to the one we obtained with Model 3 and the resulting geometry is in accordance with distorted tetrahedral coordination.

However, both models—though reasonable from the crystal chemistry point of view—imply a problem: in the high-temperature phase, the two different orbits are occupied in relation $\frac{1}{3}$. In the low-temperature phase, on the other hand, the hydrogen atoms of the $N(1)H_4^+$ tetrahedra are also distributed in two orbits but they are occupied in relation 2/2 (see also section "Comparison of the high- and low-temperature phase"). This requires that the hydrogen atoms of the two orbits in the high-temperature phase are "mixing" at the phase transition

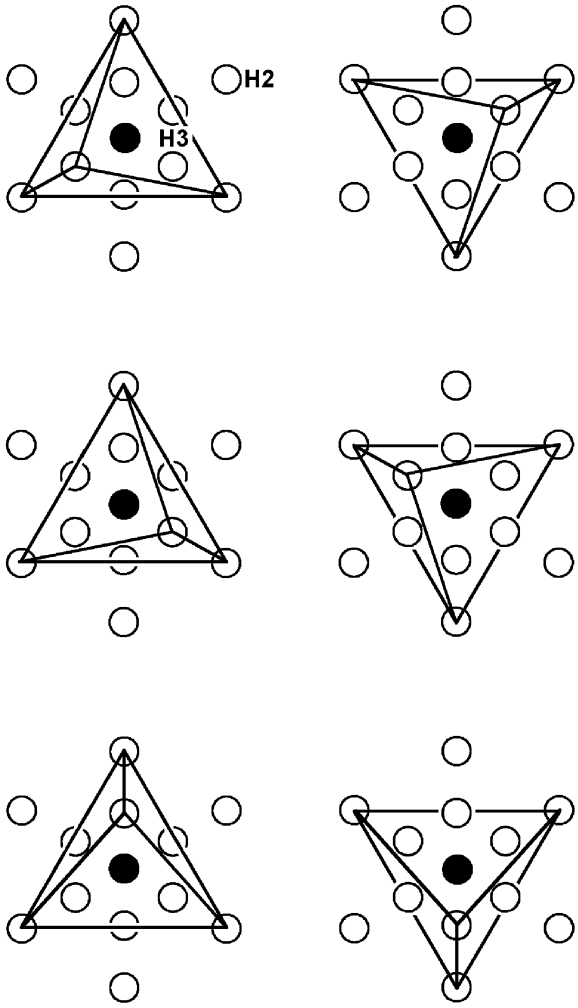

FIG. 1. The disordered $N(1)H_4^+$ tetrahedra in the high-temperature phase. Nitrogen shown as filled circle; hydrogen as open circles. The 12 possible positions of the orbits of H2 and H3 are drawn and the six possible orientations of the $N(1)H_4^+$ tetrahedra are indicated; view along [001].

and consequently, the phase transition for these hydrogen atoms is not of group–subgroup type.

A possibility of avoiding such mixing is given in model 1 i.e., the distribution of the 12 hydrogen atoms over one orbit of type 36*i*. We tried to refine the corresponding model using coordinates of positions which allow a tetrahedral coordination. However, the agreement factors were clearly worse than for the other two models and refinement of coordinates always led to positions similar to the ones which we obtained for Model 3.

5. SYMMETRY MODE ANALYSIS

Our next step is to perform symmetry mode analysis of the structural distortion relating both phases. It is necessary for the determination of the weight of the frozen primary mode which is directly related to the structural instability, and the contributions of the secondary modes which are triggered during the phase transition.

Apart from the spontaneous strain, the global distortion relating the rhombohedral structure and the distorted monoclinic one, can be described by an atomic displacement field $u_\alpha(l,k)$ representing the displacements of each atom in the low-symmetry structure. (Here, l represents the unit cell of the high-symmetry structure, k—an atomic label, and α stands for the three independent components, say x, y, z.) The displacement field is calculated from the atomic positions of the two structures expressed in relative coordinates.

The possible additional strain occurring during the phase transition can be independently derived comparing the unit cells in both phases. The rhombohedral phase, $R\bar{3}m$, with a unit cell volume of $V_{\mathrm{rho}} = 680\,\text{Å}^3$ transforms into the monoclinic phase, $C12/c1$, with $\frac{4}{3}$ the volume of the high-temperature phase ($V_{\mathrm{mcl}} = 910\,\text{Å}^3$). The lattice parameters of the rhombohedral phase at 420 K and the transformed lattice parameters of the monoclinic phase $(abc)_{\mathrm{mcl}}'$:

$$(abc)' = (abc)_{\mathrm{mcl}} \begin{pmatrix} 0 & 0 & \frac{3}{2} \\ \bar{1} & \frac{1}{2} & 0 \\ 0 & -\frac{1}{2} & \frac{1}{2} \end{pmatrix} \qquad [1]$$

are very similar: for the rhombohedral phase at 420 K the cell parameters are $a = 5.9039(5)$ Å and $c = 22.5360(6)$ Å while the transformed cell parameters for the monoclinic cell are $a = 5.904(5)$ Å and $c = 22.552(5)$ Å. In the following discussion we have, therefore, neglected the difference in cell parameters, and when referring to the *structural* or *global distortion*, we mean essentially the displacement field $u_\alpha(l,k)$, obviating the strain component.

The symmetry mode decomposition of the atomic displacements $u_\alpha(l,k)$, we are interested in, is to be performed with modes compatible with the low-symmetry $C12/c1$ structure. The primary symmetry modes transform according to the so-called *active representation* of the transition, i.e., the irreducible representation (irrep) associated with the order parameter. For the studied phase transition, the active irrep belongs to the L point of the $R\bar{3}m$-Brillouin zone (15). Its maximal invariance group (for some subspace), known also as *isotropy* group, is exactly the group of the low-symmetry phase $C12/c1$. The remaining secondary distortion components cannot produce any further symmetry break, as they are compatible with $C12/c1$-symmetry, i.e., their transformation properties are characterized by irreps of $R\bar{3}m$ which have isotropy subgroups Z that contain $C12/c1$. Hence, instead of the usual irrep description of the symmetry modes, it is possible to consider the decomposition of the total

distortion in terms of components with different isotropy space groups (16).

$$u_\alpha(l,k) = \sum_Z \sum_i C^Z(i)\phi_\alpha^Z(k,l|i). \qquad [2]$$

Here, $\phi_\alpha^Z(k,l|i)$ represent the polarization vector of a symmetry mode ϕ_i^Z, and $C^Z(i)$ the corresponding amplitude. The symmetry property that defines the modes is their compatibility with respect to the isotropy space groups Z. Hence, their derivation requires the knowledge of the chains of maximal subgroups that relate the $R\bar{3}m$ and $C12/c1$ and consequently, we call them *chain-adapted* (symmetry) modes. The polarization vectors of the symmetry modes depend only on the type of Wyckoff position to which the orbit belongs, i.e., atoms occupying orbits that belong to the same Wyckoff position and follow the same polarization vector pattern with, in general, different amplitudes.

The phase transition symmetry break $R\bar{3}m \longrightarrow C12/c1$ is of lead-phosphate type. In addition to the loss of the threefold rhombohedral axis, it involves a doubling of the unit cell. Thus, $C12/c1$ is a general subgroup of $R\bar{3}m$ of index 6. There are 12 such monoclinic subgroups of $R\bar{3}m$ distributed into four conjugate classes of three subgroups each (corresponding to the three possible orientations of the monoclinic axis with respect to the rhombohedral group; see Ref. (17) for more details). Our analysis is concerned with the conjugacy class where each subgroup is derived over one subgroup chain $R\bar{3}m > C12/m1 > C12/c1$ only, with an additional origin shift. The three monoclinic subgroups are isotropy subgroups of $L_1{}^{*-}$ (cf. Ref. (19)), i.e., the primary symmetry modes transform according to the irrep $L_1{}^{*-}$ (the irrep labels correspond to the notation used by Cracknell *et al.* (18)). In addition, there are two types of secondary modes: (i) those compatible with the $R\bar{3}m$ symmetry, and associated with the trivial Γ_1^+ (or A_{1g}) irrep of $R\bar{3}m$, and (ii) secondary modes with $C12/m1$ symmetry, also corresponding to a Brillouin zone center irrep Γ_1^+.

As a representative of the monoclinic conjugacy class, the subgroup whose bases $(\mathbf{a}, \mathbf{b}, \mathbf{c})_{\mathrm{mcl}}$ are related to that of the high-symmetry group $(\mathbf{a}, \mathbf{b}, \mathbf{c})_{\mathrm{rho}}$ by the matrix defined in Eq. [1] with an additional origin shift of $(0, -\frac{1}{4}, \frac{1}{4})$ is realized in the crystal.

The displacement field $u_\alpha(l,k)$ is determined by comparing the relative atomic coordinates of the monoclinic and rhombohedral structures. Both are referred to an auxiliary orthohexagonal cell due to its orthogonality which considerably simplifies the calculations:

$$(\mathbf{a}\,\mathbf{b}\,\mathbf{c})_{\mathrm{ort}} = (\mathbf{a}\,\mathbf{b}\,\mathbf{c})_{\mathrm{rho}} \begin{pmatrix} 1 & 1 & 0 \\ 0 & 2 & 0 \\ 0 & 0 & 1 \end{pmatrix}. \qquad [3]$$

TABLE 5
Chain-Adapted Symmetry Modes for Atoms in Wyckoff Position 6*c* and 3*a* of Space Group $R\bar{3}m$

Wyckoff position 6*c*	Primary mode ϕ_1^x	Secondary modes ϕ_2^y	ϕ_3^z	Wyckoff position 3*a*	Primary mode ϕ_4^x
	x	*y*	*z*		*x*
0 0 *z*	1	1	1	000	1
0 0 $\bar{z}$	1	−1	−1	001	−1
00z + 1	−1	1	1		
0 0 $\bar{z}$ + 1	−1	−1	−1		
Factors	$\frac{1}{2}$	$\frac{1}{2}$	$\frac{1}{2}$		

The polarization vectors are referred to the same basis. With the help of the transformation matrices (Eqs. [1] and [3]), see also the appendix) the determination of the polarization vectors in the hexagonal setting of $R\bar{3}m$ is straightforward.

In the high-temperature phase of letovicite, the atoms occupy four different types of orbits belonging to Wyckoff positions 3*a*(N1), 6*c*(S,N2,H4), 9*e*(H1), and 18*h*(O1,O2,H2,H3,H5). No symmetry modes are allowed for the *H*1 atoms. The chain-adapted modes for the rest of the occupied Wyckoff positions are given in Tables 5 and 6. Due to the doubling of the monoclinic cell, atoms belonging to two consecutive rhombohedral cells (along the trigonal axis) are considered. The modes are normalized with respect to the number of independent atoms in the two cells. For N1 atoms, there is just one primary symmetry mode along the *x* orthohexagonal axis. Along the same axis is the primary mode (ϕ_1^x) for 6*c* atoms. In addition, there are two secondary modes for these atoms: $\phi_2{}^y$, compatible with $C12/m1$, and one $R\bar{3}m$-mode ($\phi_3{}^z$). There are nine relevant modes for 18(*h*) atoms (Table 6): four $C12/c1$-primary ones ($\phi_{10}^x, \phi_{11}^y, \phi_{12}^z, \phi_{13}^x$), and five secondary including two $R\bar{3}m$ modes (ϕ_5^{xy}, ϕ_6^z), and three $C12/m1$ modes (ϕ_7^y, ϕ_8^{xy}, ϕ_9^z).

The listed chain-adapted modes ϕ_i^Z are normalized and their amplitudes $C^Z(i)$ in the total structural distortion $u_\alpha(l,k)$ are easy to determine:

$$C^Z(i) = \sum_{l,k,\alpha} u_\alpha(l,k)\phi_\alpha^Z(l,k|i). \qquad [4]$$

The values of the amplitudes $C^Z(i)$ for all atoms are listed in Table 7. The primary mode amplitudes for the atoms in 6*c* Wyckoff position (S, N2, H4) have much higher values than those of the secondary ones, including an order of magnitude for N2 atoms. However, it can also be observed that some secondary modes make significant contribution to the global atomic displacement, as in the case of the O1- and H5-atoms.

TABLE 6
Chain Adapted Symmetry Modes for Atoms in Wyckoff Position 18*h* of Space Group $R\bar{3}m$

		Secondary modes					Primary modes $C12/m1$			
		$R\bar{3}m1$		$C12/m_1$						
R-centered cell	*C*-centered cell	ϕ_5^{xy}	ϕ_6^z	ϕ_7^y	ϕ_8^{xy}	ϕ_9^z	ϕ_{10}^x	ϕ_{11}^y	ϕ_{12}^z	ϕ_{13}^x
x	$\frac{3}{2}x$	$\frac{3}{2}$			$\frac{1}{2}$		1			
$-x$	$-\frac{1}{2}x$	$-\frac{1}{2}$		1	$\frac{1}{2}$			1		
z	z		1			$\frac{1}{2}$				
x	$\frac{3}{2}x$	$\frac{3}{2}$			$\frac{1}{2}$				1	
$-x$	$-\frac{1}{2}x$	$-\frac{1}{2}$		1	$\frac{1}{2}$			1		
z	z		1			$\frac{1}{2}$		z		1
x	0									1
$2x$	x	1		1	-1					
z	z		1			-1				
$-2x$	$-\frac{3}{2}x$	$-\frac{3}{2}$			$-\frac{1}{2}$		1			
$-x$	$-\frac{1}{2}x$	$-\frac{1}{2}$		1	$\frac{1}{2}$			-1		
z	z		1			$\frac{1}{2}$			-1	
$-x$	$-\frac{3}{2}x$	$-\frac{3}{2}$			$-\frac{1}{2}$		1			
x	$\frac{1}{2}x$	$\frac{1}{2}$		-1	$-\frac{1}{2}$			1		
$-z$	$-z$		-1			$-\frac{1}{2}$			1	
$2x$	$\frac{3}{2}x$	$\frac{3}{2}$			$\frac{1}{2}$		1			
x	$\frac{1}{2}x$	$\frac{1}{2}$		-1	$-\frac{1}{2}$			-1		
$-z$	$-z$		-1			$-\frac{1}{2}$			-1	
$-x$	0									1
$-2x$	$-x$	-1		-1	1					
$-z$	$-z$		-1			1				
x	$\frac{3}{2}x$	$\frac{3}{2}$			$\frac{1}{2}$		-1			
$-x$	$-\frac{1}{2}x$	$-\frac{1}{2}$		1	$\frac{1}{2}$			-1		
$z+1$	$z+1$		1			$\frac{1}{2}$			-1	
x	0									-1
$2x$	x	1		1	-1					
$z+1$	$z+1$		1			-1				
$-2x$	$-\frac{3}{2}x$	$-\frac{3}{2}$			$-\frac{1}{2}$		-1			
$-x$	$-\frac{1}{2}x$	$-\frac{1}{2}$		1	$\frac{1}{2}$			1		
$z+1$	$z+1$		1			$\frac{1}{2}$			1	
$-x$	$-\frac{3}{2}x$	$-\frac{3}{2}$			$-\frac{1}{2}$		-1			
x	$\frac{1}{2}x$	$\frac{1}{2}$		-1	$-\frac{1}{2}$			-1		
$-z+1$	$-z+1$		-1			$-\frac{1}{2}$			-1	
$2x$	$\frac{3}{2}x$	$\frac{3}{2}$			$\frac{1}{2}$		1			
x	$\frac{1}{2}x$	$\frac{1}{2}$		-1	$-\frac{1}{2}$			-1		
$-z+1$	$-z+1$		-1			$-\frac{1}{2}$			-1	
$-x$	0									-1
$-2x$	$-x$	-1		-1	1					
$-z+1$	$-z+1$		-1			1				
Factors		$\frac{1}{2\sqrt{6}}$	$\frac{1}{2\sqrt{3}}$	$\frac{1}{2\sqrt{3}}$	$\frac{1}{2\sqrt{2}}$	$\sqrt{\frac{1}{6}}$	$\frac{1}{2\sqrt{2}}$	$\frac{1}{2\sqrt{2}}$	$\frac{1}{2\sqrt{2}}$	$\frac{1}{2}$

TABLE 7
Amplitudes $\times 10^4$ of the Symmetry Modes

	Primary	Secondary		Primary	
Atom	ϕ_1^x	ϕ_2^y	ϕ_3^z	Atom	ϕ_4^x
S	631.0	132.2	0.2	N1	383.8
N2	−500.4	−66.7	−28.1		
H4	−854.2	146.0	−70.8		

	Secondary					Primary			
Atom	ϕ_5^{xy}	ϕ_6^z	ϕ_7^y	ϕ_8^{xy}	ϕ_9^z	ϕ_{10}^x	ϕ_{11}^y	ϕ_{12}^z	ϕ_{13}^x
O1	−549.7	−16.5	75.7	−132.7	−8.3	170.6	−37.9	8.3	0.0
O2	269.8	−142.7	−386.5	−79.6	−313.6	−1064.6	143.8	313.5	−1087.2
H5	−931.5	1260.6	458.7	−291.3	−91.9	−633.7	476.9	−74.1	−1482.0

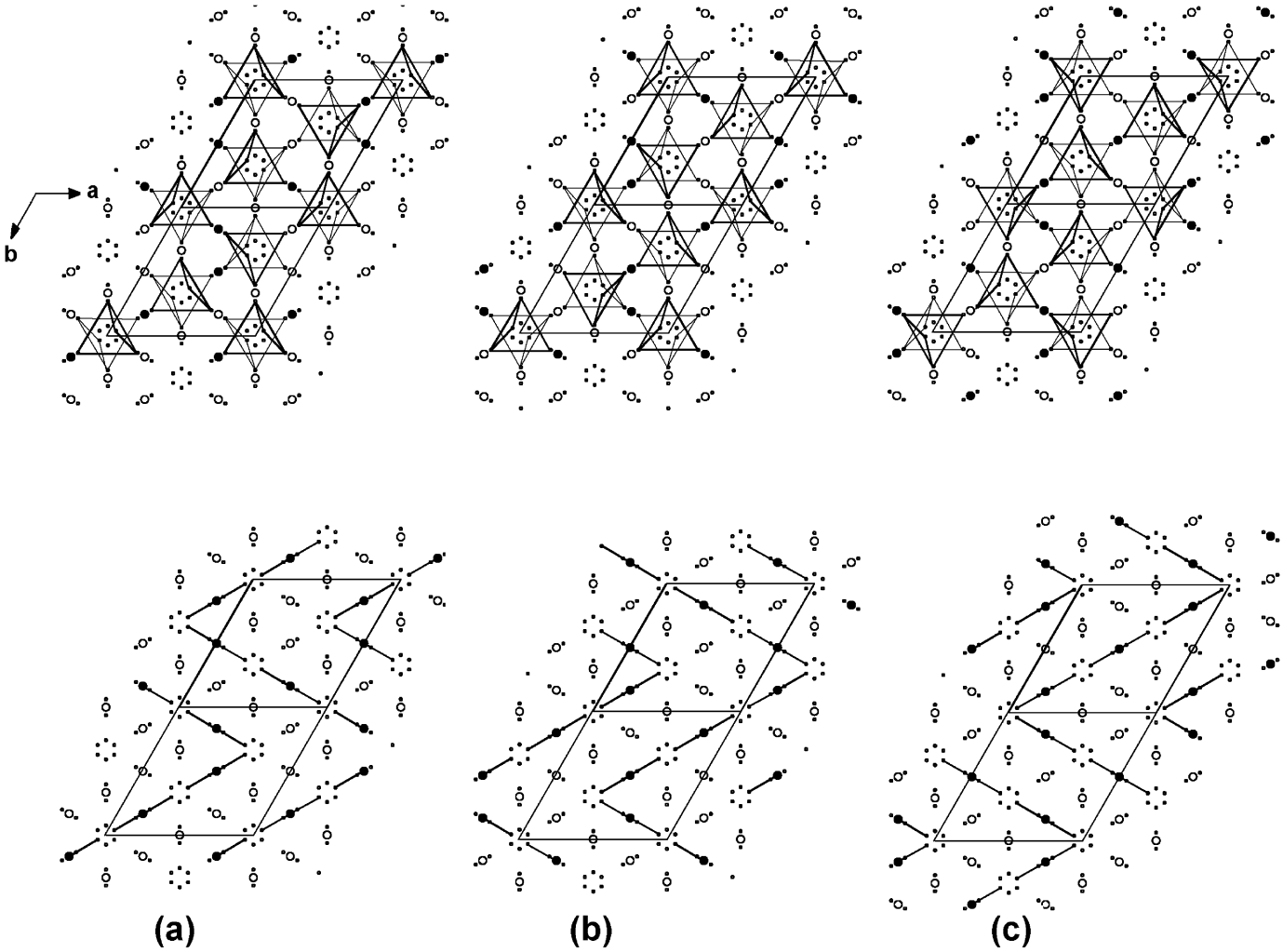

FIG. 2. Partial a_{rho}, b_{rho} projections of the structure of $(NH_4)_3H(SO_4)_2$ (a: $z_{rho} = -0.2$–0.87; b: $z_{rho} = 0.47$–1.53; c: $z_{rho} = 1.13$–2.2). Oxygen atoms shown as small circles; hydrogen atoms as large circles; Below: all possible positions of the O1 and H1-orbit in the high-temperature phase are indicated. H1-positions occupied in the low-temperature phase are shown as circles. The hydrogen bonding system of the low-temperature phase is indicated. Above: Outlines of sulfate tetrahedra in the low-temperature phase are drawn.

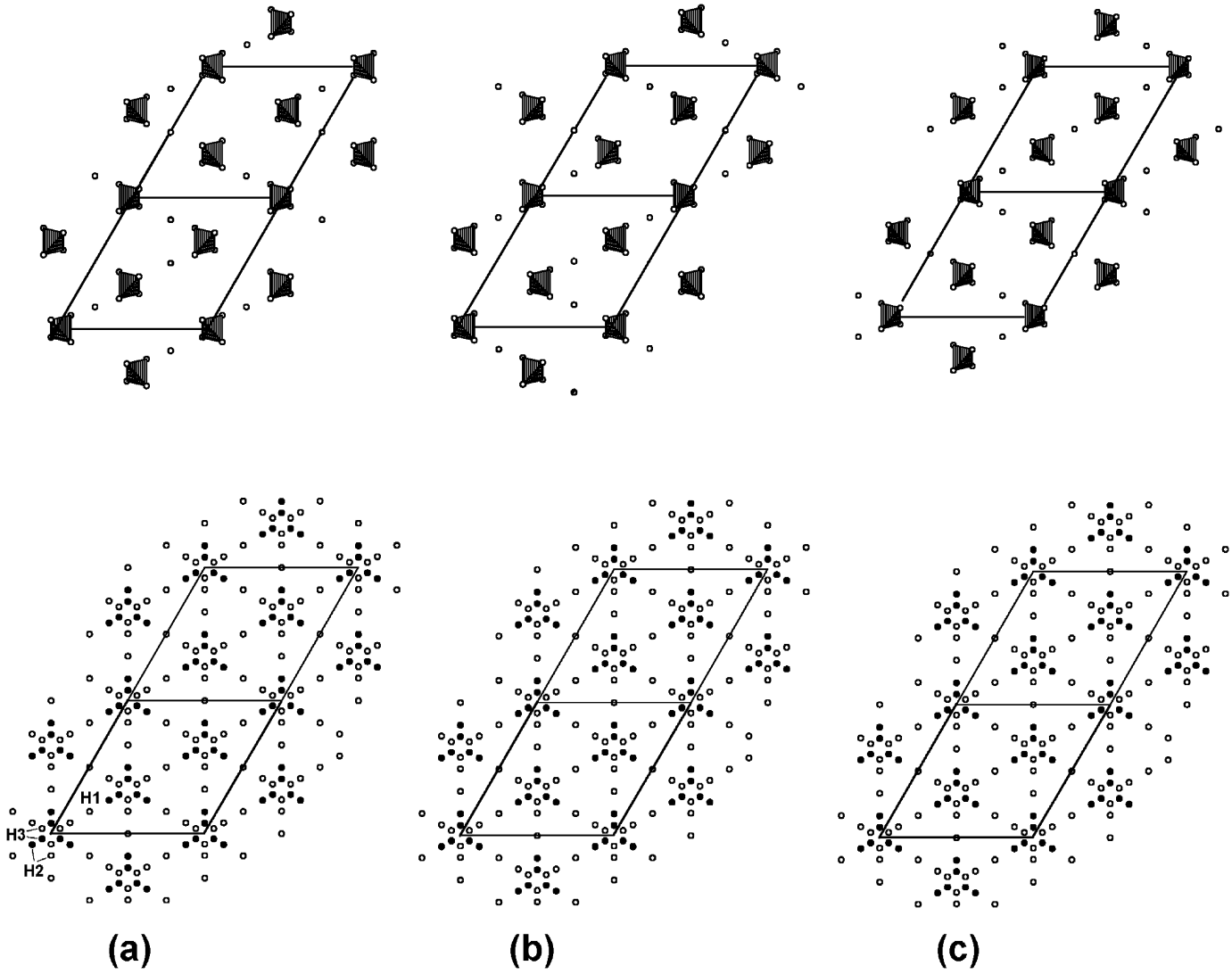

FIG. 3. Partial a_{rho}, b_{rho} projections of the structure of $(NH_4)_3H(SO_4)_2$ (a: $z_{rho} = -0.2$–0.87; b: $z_{rho} = 0.47$–1.53; c: $z_{rho} = 1.13$–2.2) Below: All possible positions of the hydrogen atoms H1–H3 in the high-temperature phase are drawn as circles. The corresponding occupied positions of the low-temperature phase (after transformation of the coordinates) have been filled. Above: the same partial projection of the low-temperature phase; now $N(1)H_4^+$ tetrahedra are shown. Notice that for periodicity z_{rho} has to reach up to 2.

6. COMPARISON OF THE HIGH- AND LOW-TEMPERATURE PHASE

Figures 2–4 illustrate the relationship between the high- and low-temperature phase. Figure 2 gives three partial a_{rho},b_{rho}-projections with (a) $z_{rho} = -0.2$–0.87; (b) $z_{rho} = 0.47$–1.53 and (c) $z_{rho} = 1.13$–2.2 of the structures taking into account only the oxygen atoms and the hydrogen H(1).[3] Large circles represent H(1) atoms, small circles represent oxygen atoms. All possible positions of H(1) and O(1) in the high-temperature phase are drawn, but only H(1) positions which are occupied in the low-temperature phase have been filled in black. The hydrogen bonds observed in the low-temperature phase are schematically drawn as lines in the projections of the bottom. In the projections of the top, the sulfate tetrahedra realized in the low-temperature phase are indicated. Only oxygen positions which form part of this tetrahedra are occupied in the low-temperature phase.

The occupations of the possible positions O(1) and H(1) are coupled in such a way that the zig-zag-like pattern for the hydrogen bonds which can be observed in the figure is formed. The orbit of Wyckoff position 9*e* where the H(1) atoms are located in the high-temperature phase splits into 3 orbits 4*e*, 4*a,* and 4*b* of space group $C12/c1$. It is

[3]To obtain a periodical arrangement for the monoclinic phase it is necessary to take into account two rhombohedral unit cells in direction of b_{rho} and c_{rho}.

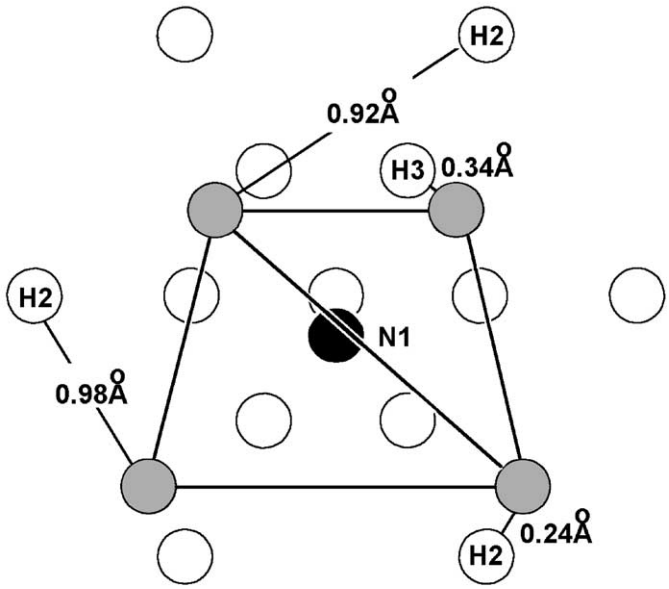

FIG. 4. The $N(1)H_4^+$ tetrahedra in the high- and low-temperature phase.

remarkable that this splitting involves no additional displacement of the atoms. Of the three possible orbits only the 4*a* position (corresponding to coordinates 0,0,0; 0,0, $\frac{1}{2}$; $\frac{1}{2}$, $\frac{1}{2}$, 0; $\frac{1}{2}$, $\frac{1}{2}$, $\frac{1}{2}$) is occupied in the monoclinic phase while the other two orbits are left empty. For the disordered O(1) something similar is observed. The 18*h* orbit of the high-temperature phase splits into three orbits of general position 8*f* in the low-temperature phase. Yet, the O(1) atoms order over the positions of one of these orbits only and leave the other two orbits unoccupied. For these atoms, however, one also observes an additional displacement.

The symmetry mode analysis which we carried out to describe the structural distortion characterizing the phase transition yields reasonable results (see Table 7). Usually, we expect the amplitudes of the primary modes to be greater than the corresponding amplitudes of the secondary modes and this clearly holds for the atoms S, N1, N2 and O2. However, the amplitude for one of the secondary modes of atom O1 is surprisingly three times greater than the largest amplitude of the primary modes ($\Phi_5^{xy} = -549.7$ compared to $\Phi_{10}^{x} = 170.6$). Yet of course, for this atom one has to take into account the fact that there is also the above-mentioned order/disorder component which determines its behavior in the phase transition. Even for the two hydrogen atoms H4 and H5, one observes that the amplitudes of the primary modes are generally more important than the corresponding secondary modes despite the fact that errors in coordinates are naturally rather big.

Figure 3 is an identical projection as of Fig. 2 and illustrates the situation for the $N(1)H_4^+$ tetrahedra in the high- and low-temperature phase. Below the possible positions of the hydrogen atoms H(1), H(2) and H(3) in the high-temperature phase are drawn as open circles while the occupied positions of the ordered low-temperature phase are filled in black. In the above diagrams, the low-temperature phase with the corresponding $N(1)H_4^+$ tetrahedra and the hydrogen atoms of the hydrogen bonds are drawn.

Figure 4 shows the $N(1)H_4^+$ tetrahedra in high- and low-temperature phase in more detail. The position of the N(1) atom in the low-temperature phase is shown as a filled circle, the positions of the ordered hydrogen atoms in the monoclinic phase are indicated as gray circles. Positions belonging to the orbits of N(1), H(2) and H(3) of the high-temperature phase are open circles. The choice of one of the six positions of the orbit of H(3), together with a small displacement of 0.34 Å leads to the position of one of the hydrogens of the low-temperature phase. The second hydrogen of the tetrahedra in the low-temperature phase can be described as resulting from one of the six possible positions from the orbit H(2) and also needs only a rather small displacement of the atom of 0.24 Å. Anyhow, with the two positions chosen in the high-temperature phase the other two hydrogen atoms of the tetrahedra in the rhombohedral phase are also defined (they are marked as H2). If one assumes that no bonds within the NH_4^+ tetrahedra are broken, this necessarily means that the displacement of the other two remaining H-atoms are rather big (0.92 and 0.98 Å), respectively.[4]

In this context, it is remarkable that 1H NOESY experiments indicate a chemical exchange between ammonium and acidic protons in the high-temperature phase (19). This observation in combination with our results mentioned above suggests that the protons involved in this exchange are the H2 and H3 ions which constitute the tetrahedra around the N1 atom while the hydrogen ions of the $N(2)H_4$ tetrahedra most probably do not participate in the protonic conductivity.

APPENDIX

Transformation matrices

$$\begin{pmatrix} x \\ y \\ z \end{pmatrix}_{\text{rho}} = \left(\begin{array}{ccc|c} \frac{1}{3} & \bar{1} & \bar{1} & 0 \\ \frac{2}{3} & 0 & \bar{2} & -\frac{1}{2} \\ \frac{2}{3} & 0 & 0 & 0 \end{array}\right) \begin{pmatrix} x \\ y \\ z \end{pmatrix}_{\text{mcl}},$$

$$\begin{pmatrix} x \\ y \\ z \end{pmatrix}_{\text{ort}} = \left(\begin{array}{ccc|c} 1 & -\frac{1}{2} & 0 & 0 \\ 0 & \frac{1}{2} & 0 & -\frac{1}{2} \\ 0 & 0 & 0 & 0 \end{array}\right) \begin{pmatrix} x \\ y \\ z \end{pmatrix}_{\text{rho}},$$

[4]The refined coordinates corresponding to Model 2 display a similar picture and also yield large shifts.

$$\begin{pmatrix} x \\ y \\ z \end{pmatrix}_{\text{ort}} = \left(\begin{array}{ccc|c} 0 & \bar{1} & 0 & \frac{1}{4} \\ \frac{1}{3} & 0 & \bar{1} & -\frac{1}{4} \\ \frac{2}{3} & 0 & 0 & 0 \end{array}\right) \begin{pmatrix} x \\ y \\ z \end{pmatrix}_{\text{mcl}},$$

$$(a \quad b \quad c)_{\text{rho}} = (a \quad b \quad c)_{\text{mcl}} \left(\begin{array}{ccc|c} 0 & 0 & \frac{3}{2} & 0 \\ \bar{1} & \frac{1}{2} & 0 & \frac{1}{4} \\ 0 & -\frac{1}{2} & \frac{1}{2} & -\frac{1}{4} \end{array}\right),$$

$$(a \quad b \quad c)_{\text{ort}} = (a \quad b \quad c)_{\text{rho}} \left(\begin{array}{ccc|c} 1 & 1 & 0 & 0 \\ 0 & 2 & 0 & 0 \\ 0 & 0 & 1 & 0 \end{array}\right),$$

$$(a \quad b \quad c)_{\text{ort}} = (a \quad b \quad c)_{\text{mcl}} \left(\begin{array}{ccc|c} 0 & 0 & \frac{3}{2} & 0 \\ \bar{1} & 0 & 0 & \frac{1}{4} \\ 0 & \bar{1} & \frac{1}{2} & -\frac{1}{4} \end{array}\right).$$

ACKNOWLEDGMENTS

The authors gratefully acknowledge financial support by the Deutsche Forschungsgemeinschaft (Fr1332/2-1).

REFERENCES

1. K. Gesi, *Phys. Stat. Sol. A* **33,** 479–482 (1976).
2. K. Gesi, *J. Phys. Soc. Jpn.* **43,** 1941–1948 (1977).
3. K. Gesi, *Jpn. J. Appl. Phys.* **19,** 1051–1053 (1980).
4. T. Fukami, K. Tobaru, K. Kaneda, K. Nakasone, and K. Furukawa, *J. Phys. Soc. Jpn.* **63,** 2006–2007 (1994).
5. R. H. Chen, L.-M. Wang, and S. Yang, *Phase Transitions* **37,** 141–147 (1992).
6. M. Kamouni, M. H. B. Ghozlen, and A. Daoudi, *Phase Transitions* **9,** 147–252 (1987)
7. S. Suzuki and Y. Makita, *Acta Crystallogr. B* **34,** 732–735 (1978).
8. A. Leclaire, M. Ledesert, J. C. Monier, A. Daoud, and M. Damak, *Acta Crystallogr. B* **41,** 209–213 (1985).
9. L. Schwalowsky, V. Vinnichenko, A. Baranov, U. Bismayer, B. Merinov, and G. Eckold, *J. Phys.: Condens. Matter* **10,** 3019–3027 (1998).
10. T. Fukami, K. Horiuzi, K. Nakasone, and K. Furukawa, *Jpn. J. Appl. Phys.* **35,** 2253–2254 (1996).
11. K. Sooryanarayana and T. N. G. Row, *Phase Transitions* **58,** 263–271 (1996).
12. H. Böhm, *J. Appl. Cryst.* **28,** 357 (1995).
13. K. V. K. Rao, S. V. N. Naidu, and K. S. Murthy, *J. Phys. Chem. Solids* **29,** 245–248 (1968).
14. G. Sheldrick, SHELXL97, "A Program for Refining Crystal Structures, Computer Program." University of Göttingen, Germany, 1997.
15. J. Torres, *Phys. Stat. Sol. B* **71,** 141–150 (1975).
16. M. Aroyo and J. M. Pérez-Mato, *Acta Crystallogr. A* **54,** 19–30 (1998).
17. C. Paulmann, U. Bismayer, and M. I. Aroya, *Phase Transitions* **67,** 1–26 (1998).
18. A. P. Cracknell, B. L. Davies, S. C. Miller, and W. F. Love, "Kronecker Product Tables," Vol. 1, General Introduction and Tables of Irreducible Representations of Space Groups. IFI/Plenum, New York, 1979.
19. M. Fechtelkord, A. Engelhardt, J.-C. Buhl, L. Schwalowsky, and U. Bismayer, *Sol. State Nucl. Mag. Resonance* **17,** 76–88 (2000).